

Radio–Optical–Gamma-Ray properties of MOJAVE AGN detected by Fermi/LAT ^{*}

T.G. Arshakian^{1,2}, J. León-Tavares³, M. Böttcher⁴, J. Torrealba⁵, V.H. Chavushyan⁵, M.L. Lister⁶, E. Ros^{7,1}, and J.A. Zensus¹

¹ Max-Planck-Institut für Radioastronomie, Auf dem Hügel 69, 53121 Bonn, Germany
e-mail: tarshakian@mpifr-bonn.mpg.de

² Byurakan Astrophysical Observatory, Byurakan 378433, Armenia and Isaac Newton Institute of Chile, Armenian Branch
³ Aalto University Metsähovi Radio Observatory, Metsähovintie 114, FIN-02540, Kylmälä, Finland
e-mail: leon@kurp.hut.fi

⁴ Astrophysical Institute, Department of Physics and Astronomy, Ohio University, Athens, OH 45701, USA
e-mail: boettchm@ohio.edu

⁵ Instituto Nacional de Astrofísica Óptica y Electrónica, Apartado Postal 51 y 216, 72000 Puebla, Pue, México
e-mail: [cjanet,vahram]@inaoep.mx

⁶ Department of Physics, Purdue University, 525 Northwestern Avenue, West Lafayette, IN 47907, USA
e-mail: mlister@purdue.edu

⁷ Departament d’Astronomia i Astrofísica, Universitat de València, E-46100 Burjassot, Spain
e-mail: eduardo.ros@uv.es

Received jdatej / Accepted jdatej

ABSTRACT

Aims. We use a sample of 83 core-dominated active galactic nuclei (AGN) selected from the MOJAVE (Monitoring of Jets in AGN with VLBA Experiments) radio-flux-limited sample and detected with the *Fermi* Large Area Telescope (LAT) to study the relations between non-simultaneous radio, optical, and γ -ray measurements.

Methods. We perform a multi-band statistical analysis to investigate the relations between the emissions in different bands and reproduce these relations by modeling of the spectral energy distributions of blazars.

Results. There is a significant correlation between the γ -ray luminosity and the optical nuclear and radio (15 GHz) luminosities of blazars. We report a well defined positive correlation between the γ -ray luminosity and the radio-optical loudness for quasars and BL Lacertae type objects (BL Lacs). A strong positive correlation is found between the radio luminosity and the γ -ray-optical loudness for quasars, while a negative correlation between the optical luminosity and the γ -ray-radio loudness is present for BL Lacs. Modeling of these correlations with a simple leptonic jet model for blazars indicates that variations of the accretion disk luminosity (and hence the jet power) is able to reproduce the trends observed in most of the correlations. To reproduce all observed correlations, variations of several parameters, such as the accretion power, jet viewing angle, Lorentz factor, and magnetic field of the jet, are required.

Key words. galaxies: active – galaxies: jets – radio continuum: galaxies – quasars: general – gamma rays: galaxies

1. Introduction

Blazars are observed over a wide range of the electromagnetic spectrum from radio to very-high-energy (VHE) γ -rays. Synchrotron emission, which is believed to be dominant in the radio band, originates in the relativistic bipolar outflows which on milliarsecond scales (parsec scales) appear as moving superluminal radio knots, which can be

probed by very-long-baseline interferometry (VLBI) images (e.g., Kellermann et al. 1998).

One quarter of all AGN of the radio-flux-limited MOJAVE (Lister et al. 2009a) sample objects were detected by the *Fermi* LAT during the first three months of operation (Lister et al. 2009b). For this sample of 31 blazars a significant correlation between radio (VLBA¹) flux density at 15 GHz and γ -ray photon flux was reported for quasi-simultaneous radio – γ -ray measurements

^{*} Table 4 is only available in electronic form at the CDS via anonymous ftp to cdsarc.u-strasbg.fr (130.79.128.5).

¹ Very Long Baseline Array

(Kovalev et al. 2009). They suggested that the radio and γ -ray emissions are produced in the cores of parsec-scale jets. A positive correlation between radio flux density at 8.4 GHz and γ -ray flux was reported by Linford et al. (2011) for 50 flat-spectrum quasars selected from the VLBA Imaging and Polarimetry Survey (VIPS). The correlation appeared to be stronger for radio bright quasars and the differences between the γ -ray loud and quiet flat-spectrum quasars can be explained by Doppler boosting. Strong correlation between the γ -ray flux (above 100 MeV) and the 20 GHz flux density was found for 134 flat-spectrum quasars and BL Lacs which were identified from cross correlation of the 1FGL with the 20 GHz Australia Telescope Compact Array radio survey catalogue (Mahoni et al. 2010, Ghirlanda et al. 2011). Pushkarev et al. (2010) studied 187 blazars selected from the First *Fermi* LAT catalog (1FGL; Abdo et al. 2010b) and found that on average the γ -ray flares precede the radio flares at 15 GHz with intrinsic time delays of 1.2 months. This result suggests that the origin of the bulk of the the γ -ray photons is located within the 15 GHz VLBI core. High-frequency VLBI (43 GHz) and multi-waveband monitoring of blazars indicate that a single superluminal radio knot can cause a number of γ -ray flares, and that very rapid variability of γ -ray emission comes near the location of the 43 GHz cores of blazars jets (Marscher & Jorstad 2010). Recently, León-Tavares et al. (2011) have shown that the strongest γ -ray flares follow the *mm* flares in about 70 days. They interpret this as strong γ -ray events being produced at a distance of several parsecs downstream of the *mm*-wave core.

The MOJAVE blazars show a tight connection between radio VLBA and optical emission. Long-term radio – optical monitoring of radio galaxies showed that a variable optical emission on scales from a few months to a few years is generated in the innermost 0.4 pc region of the radio jet (Arshakian et al. 2010a; León-Tavares et al. 2010). A significant positive correlation at milliarcseconds scales was reported between the optical nuclear emission and (i) the radio emission of the unresolved cores at 15 GHz in superluminal quasars, and (ii) the extended jet emission in BL Lac objects by Arshakian et al. (2010b). Those results suggested that the radio and optical emissions are beamed and originate in the innermost part of the sub-parsec-scale jet in quasars.

Extreme optical variability was a clear signature for some blazars detected at γ -ray energies during the *CGRO*/EGRET era (Fichtel et al. 1994). Taking advantage of the improved gamma sensitivity of *Fermi*/LAT, recent multiwavelength variability studies on individual sources have confirmed the tight connection among the γ -ray and variable optical emission (e.g., 3C 273 in Abdo et al. 2010a).

So far there was no attempt to compare optical continuum properties among γ -ray blazars. In this manuscript we study multi-band correlations to investigate the single production mechanism for continuum emission in different wavebands. Taking advantage of the unprecedented

sensitivity provided by the 1FGL, we analyze relations between optical nuclear emission, radio emission on scales of milliarcseconds, and γ -ray emission of more than 80 MOJAVE AGN that had high confidence *Fermi*/LAT source associations after its first 11 months of operation. As discussed in Abdo et al. (2010b), it is possible that some blazars may lack a *Fermi*/LAT association due their location in a particularly confused location (numerous γ -ray sources, or high diffuse background near the galactic plane). Since the MOJAVE sample includes only very radio-bright sources and avoids the galactic plane region, we will refer for convenience in this paper to the non-LAT associated MOJAVE sources as 'non-detected'. An interpretation of the correlations and the main physical process driving these correlations is discussed in the framework of a steady-state jet model.

The sample of blazars is defined in Sect. 2. In Sect. 3, the Kendall's τ statistical test is used to examine the correlations between emission characteristics defined in radio, optical, and γ -ray regimes. We interpret the implications of the jet model in Sect. 4 and summarize our results in Sect. 5.

Throughout the paper a flat cosmology with $H_0 = 71$ km s⁻¹ Mpc⁻¹, $\Omega_m = 0.27$, and $\Omega_\Lambda = 0.73$ is adopted.

2. The sample of AGN detected with *Fermi*/LAT

We study a statistically complete sample of 135 core-dominated AGN compiled from the MOJAVE sample and the VLBA 15 GHz monitoring survey (Kellermann et al. 1998; Zensus et al. 2002; Lister et al. 2009a). The complete sample, MOJAVE-1, is limited by the total VLBA (mas-scale) flux density at 15 GHz: it is greater than 1.5 Jy for sources in the Northern hemisphere ($\delta > 0$) and > 2 Jy in the Southern hemisphere ($-20 < \delta < 0$). The sample comprises quasars, BL Lacs, radio galaxies and some unidentified sources having typically a core-jet structure on milliarcsecond scales. At high redshifts, the sample has a selection bias towards BL Lacs and quasars with fast and bright one-sided jets oriented closer to the line of sight, while at low redshifts ($z < 0.1$) there is a selection bias towards slow and intrinsically bright jets of radio galaxies (for more details see Lister & Homan 2005, Arshakian et al. 2010b).

The 1FGL catalogue includes 83 sources from the MOJAVE-1 sample (hereafter, M1-1FGL sample): 59 quasars, 19 BL Lacs, 3 radio galaxies, and 2 unidentified sources. Most of the blazars not detected at γ -ray energies come from the weaker radio portion of the MOJAVE-1 sample (Fig. 1) indicating that the γ -ray selected sample is biased towards radio strong blazars. The latter also are strong γ -ray blazars since there is a strong positive correlation between radio and γ -ray fluxes of blazars (Kovalev et al. 2009).

For these 83 γ -ray selected sources, optical nuclear fluxes and redshift measurements were available for 76 objects (Arshakian et al. 2010b): 58 quasars, 15 BL Lacs, and 3 radio galaxies (see Table 4). A procedure to correct

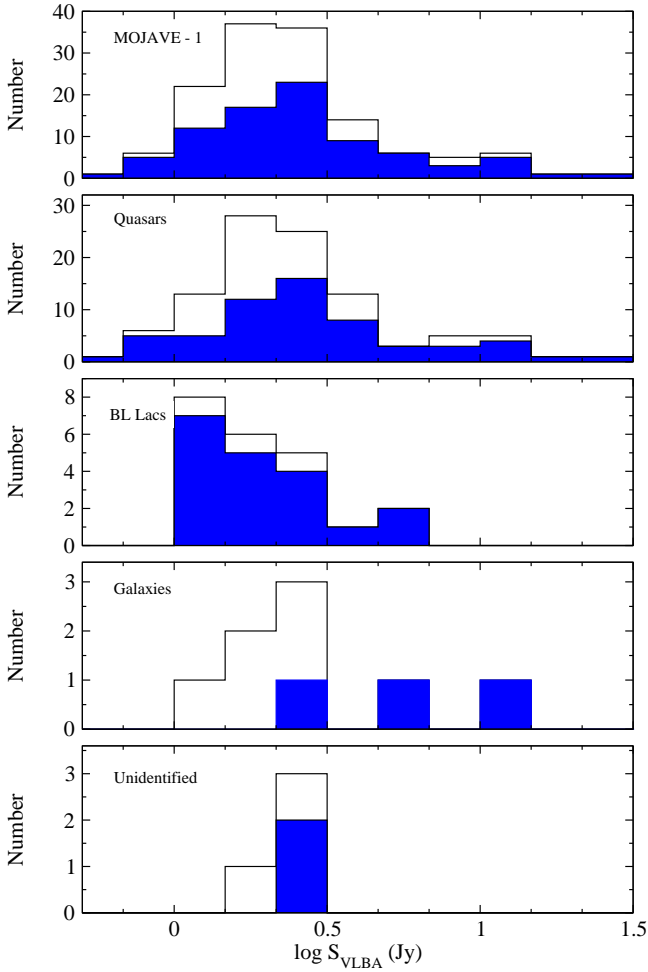


Fig. 1 Distribution of radio VLBA flux densities at 15 GHz for 135 MOJAVE-1 AGN (full line) and AGN detected with *Fermi*/LAT (filled blue histogram) for all blazars, quasars, BL Lacs, radio galaxies, and optically unidentified sources.

the photometric fluxes for a stellar emission is discussed in Arshakian et al. (2010b). Typical errors associated with optical nuclear fluxes are between 15% and 25%.

We derive the optical nuclear luminosities (L_{opt}), total VLBA luminosities (L_{VLBA}), and the rest frame radio-optical loudness (the ratio of the K -corrected radio and optical fluxes, $R = S'_{\text{VLBA}}/S'_{\text{opt}} = S_{\text{VLBA}}(1+z)^{-\alpha_r+\alpha_o}/S_{\text{opt}}$, where $\alpha_r = 0$ is the spectral index of the total VLBA component, α_o is the optical spectral index adopted to be -0.5). We use the optical nuclear fluxes at 5100 \AA given in Arshakian et al. (2010b) and the total radio flux densities at 15 GHz measured (during the period from 1994 to 2003 as part of the VLBA 15 GHz monitoring survey) at the epochs at which the unresolved component flux density has its maximum value. γ -ray luminosities were computed using the Eq. (1) in Ghisellini et al. (2009),

$$L_\gamma = 4\pi d_L^2 \frac{S_\gamma(\nu_1, \nu_2)}{(1+z)^{1-\alpha_\gamma}}, \quad (1)$$

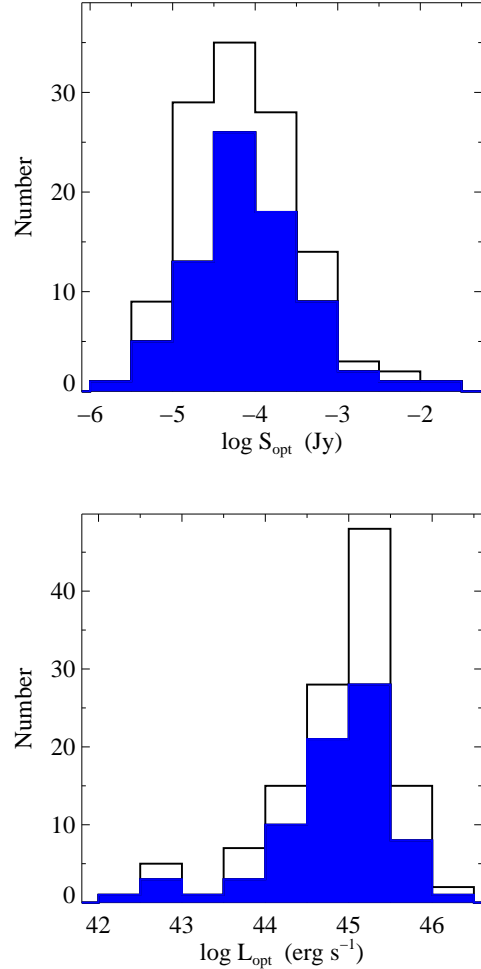


Fig. 2 Distributions of optical nuclear fluxes (top panel) and luminosities (bottom panel) at 5100 \AA for 122 AGN from the MOJAVE-1 sample (full line). Among these, 76 AGN are detected as the gamma-ray source (filled histogram) with *Fermi*/LAT during the 1FGL period.

where $S_\gamma(\nu_1, \nu_2)$ is the energy flux between $\nu_1 = 0.1 \text{ GeV}$ and $\nu_2 = 100 \text{ GeV}$ from the 1FGL catalogue, α_γ is the γ -ray energy index between the frequencies ν_1 and ν_2 , and d_L is the luminosity distance. Note that the γ -ray, optical, and radio luminosities of the MOJAVE-1 blazars are estimated from non-simultaneous observations and their typical uncertainties are between $\sim (10 - 15)\%$ in γ -ray band, $\sim (15 - 25)\%$ in optical, and $\lesssim 5\%$ (Kovalev et al. 2005) in radio band. The rest frame γ -ray-radio loudness is defined as $G_r = S'_\gamma/S'_{\text{VLBA}} = S_\gamma(1+z)^{-\alpha_\gamma+\alpha_r}/S_{\text{VLBA}}$ and the γ -ray-optical loudness is $G_o = S'_\gamma/S'_{\text{opt}} = S_\gamma(1+z)^{-\alpha_\gamma+\alpha_o}/S_{\text{opt}}$.

We use the non-parametric Kendall's τ test to analyze correlations between independent variables and the partial Kendall's τ test (Akritas & Siebert 1996) to account for the common dependence on redshift in the correlations between luminosities. Throughout the paper we assume a

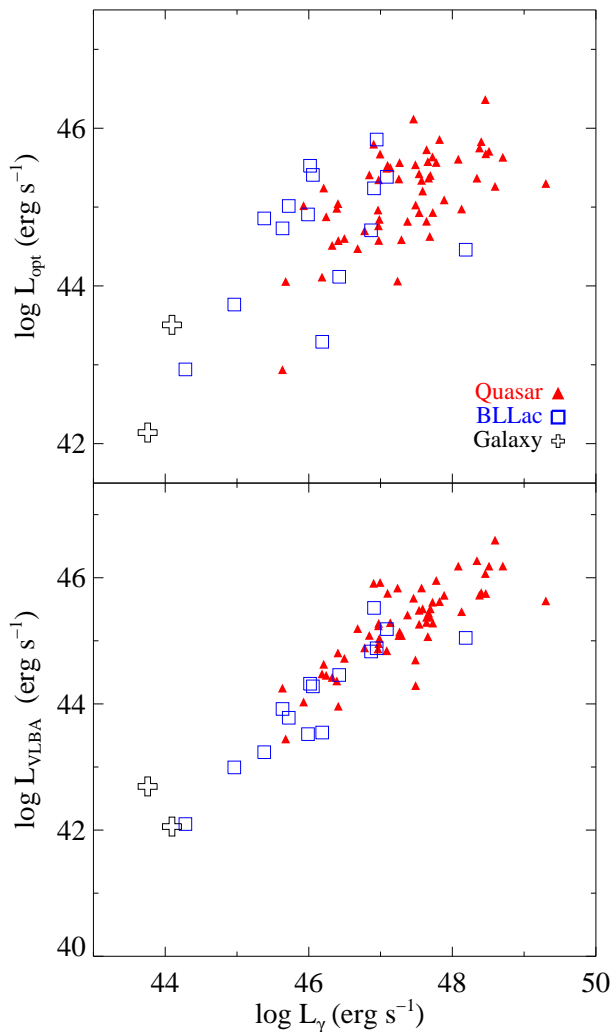


Fig. 3 Optical nuclear luminosity against γ -ray luminosity (top panel), and radio VLBA (15 GHz) luminosity against γ -ray luminosity (bottom panel) for AGN from the M1-1FGL sample. Labels in the top panel denote the corresponding population.

correlation to be significant if the chance probability for a null hypothesis is $P < 0.05$.

3. Relations between γ -ray, optical, and radio properties of superluminal AGN

Detection rate of γ -ray blazars. The relative number of blazars detected in γ -rays increases with increasing radio flux, and most quasars not detected in γ -rays are radio weak (Fig. 1). This is explained by a tight correlation between radio and γ -ray emission of quasars (Kovalev et al. 2009). Most of BL Lacs and radio bright galaxies are detected in γ -ray band.

The distributions of optical nuclear fluxes for detected and not detected γ -ray blazars have similar ranges (Fig. 2; top panel). The Kolmogorov-Smirnov (K-S) statistical test shows that the null hypothesis that these distributions

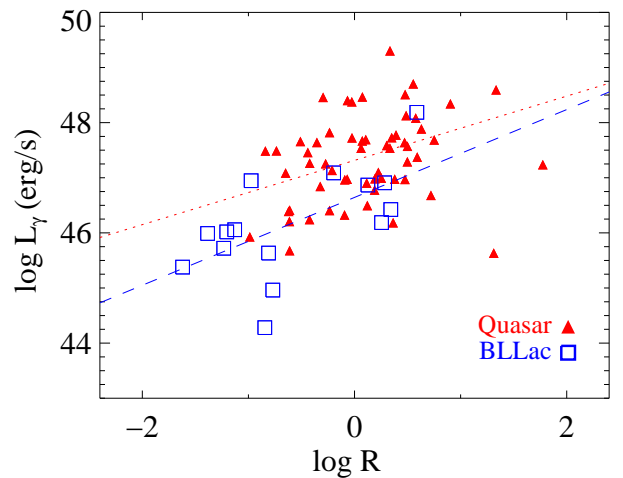


Fig. 4 γ -ray luminosity (L_γ) versus radio-optical loudness ($R \equiv S'_{VLBA}/S'_{opt}$) for the M1-1FGL quasars and BL Lacs. The dotted and dashed lines represent the ordinary least-square fit to the data for quasars and BL Lacs respectively.

are drawn from the same parent population can not be rejected ($P = 0.15$; confidence level of 85 %). We conclude that among radio-selected blazars, the detection rate of γ -ray AGN does not depend on their optical nuclear fluxes, and most of undetected γ -ray blazars are in fact quite optically luminous (Fig. 2; bottom panel).

Optical – Radio emission. Arshakian et al. (2010b) found a positive correlation in the $L_{opt} - L_{VLBA}$ plane for AGN from the MOJAVE-1 sample. They concluded that the correlation is due to the population of quasars and that the optical emission is non-thermal and generated in the parsec-scale jet. This is supported by studies of individual radio galaxies, 3C 390.3 and 3C 120 (Arshakian et al. 2010a; León-Tavares et al. 2010) for which a link between optical continuum variability and kinematics of the parsec-scale jet was found. It was interpreted in terms of optical continuum flares generated at subparsec-scales in the innermost part of a relativistic jet rather than in the accretion disk.

Gamma-ray – Optical emission. No correlation is found for BL Lacs, while a significant positive correlation between L_γ and L_{opt} is found for quasars (99%; Fig. 3; Table 1) suggesting a single production mechanism for γ -ray and optical nuclear emission.

Gamma-ray – Radio emission. Kovalev et al. (2009) reported a correlation between γ -ray and radio VLBA (8 GHz) emission for a sample of ~ 30 AGN. This correlation holds at high confidence level ($> 99.9\%$; Fig. 3) for non-simultaneous measurements at 15 GHz and a larger sample (M1-1FGL) of AGN. This suggests that the powers averaged over the long time scales are correlated and, hence, the Doppler-factors of the parsec-scale jet in the gamma and radio domains are not changing substantially on a timescale of a few years. Pushkarev et al. (2010)

Table 1 Kendall’s τ correlation analysis between emission characteristics of AGN from the M1-1FGL sample. A1 and A2 are the independent variables for which the Kendall’s τ correlation analysis is performed, and A3 is the control variable (if exists then the partial Kendall’s τ correlation analysis is applied to A1 and A2), τ is the correlation coefficient, and P is the probability of a chance correlation. The correlations are considered to be significant if the chance probability $P < 0.05$ (or confidence level $> 95\%$).

A1	A2	A3	All		Quasars		BL Lacs	
			τ	P	τ	P	τ	P
L_{VLBA}	L_{opt}	z	0.22	0.004	0.25	0.006	0.01	0.957
L_{γ}	L_{opt}	z	0.19	0.015	0.23	0.011	0.03	0.899
L_{γ}	L_{VLBA}	z	0.41	2×10^{-7}	0.39	2×10^{-5}	0.42	0.036
L_{γ}	$S'_{\text{VLBA}}/S'_{\text{opt}}$	-	0.36	4×10^{-6}	0.24	0.008	0.43	0.025
L_{VLBA}	$S'_{\gamma}/S'_{\text{opt}}$	-	0.41	2×10^{-7}	0.34	0.0002	0.16	0.4
L_{opt}	$S'_{\gamma}/S'_{\text{VLBA}}$	-	-0.11	0.11	0.16	0.071	-0.39	0.042

found that the γ -ray emission leads the radio emission of the parsec-scale jet at 15 GHz with a time delay of a few months. They interpreted the observed time lag as a result of synchrotron opacity in the jet: the radio and γ -ray emissions can be generated in the same region by perturbations of the jet (Marscher & Gear 1985) and become observable with some time delay due to the opacity effects. If this scenario is correct, the variable optical emission is also generated in the perturbation moving upstream in the jet, and one should expect that the optical emission leads the radio emission and is also delayed with respect to the γ -ray emission.

The $L_{\text{VLBA}} - L_{\gamma}$ correlation is visibly tighter (0.39 dex scatter) than the $L_{\text{opt}} - L_{\gamma}$ one (0.54 dex scatter; Fig. 3). The remarkably tight relation between L_{VLBA} and L_{γ} , $\log L_{\text{VLBA}} = (0.83 \pm 0.03) \log L_{\gamma} + (5.96 \pm 0.26)$, over a range of about five orders of magnitudes, can be used to estimate the γ -ray flux of not detected γ -ray blazars from their VLBA flux density. One may think that the corrected optical nuclear emission of some AGN (Arshakian et al. 2010b) might be contaminated by a contribution of a stellar component, thus causing the large dispersion in the $L_{\text{opt}} - L_{\gamma}$ diagram. This contamination should be stronger in radio galaxies and weaker in quasars and BL Lacs for which the contribution of optical nuclear emission is dominant. The large dispersion in the $L_{\text{opt}} - L_{\gamma}$ plane can be due to stronger variability in the optical regime than in the radio, and/or a wider range of Doppler factors in the optical regime compared to the range of Doppler factors of the jet at the location where the 15 GHz emission is produced, if the bulk of the optical emission is generated in the relativistic jet and it is Doppler boosted.

We report a significant positive correlation ($> 99\%$) between L_{γ} and radio-optical loudness R for quasars and BL Lacs (see Fig. 4 and Table 1). For the combined sample the $L_{\gamma} \propto R^{0.95 \pm 0.11}$, for quasars $L_{\gamma} \propto R^{0.44 \pm 0.18}$, and for BL Lacs $L_{\gamma} \propto R^{0.79 \pm 0.27}$. The slope derived for quasars is shallower than for BL Lacs. To test the robustness of this result, we excluded one outlier quasar ($\log R = 1.31$ and $\log L_{\gamma} = 45.63$) and repeated the fitting of data. The slope for quasars increases, 0.58 ± 0.17 , and coincides with

the slope of BL Lac objects within the error range. We conclude that the slopes for quasars and BL Lacs are not statistically different. A noticeable difference in radio-optical loudness is found between populations of quasars and BL Lacs: $\log R = 0.12$ for quasars and $\log R = -0.81$ for BL Lacs.

Gamma-ray loudness. We define the rest frame γ -optical loudness (G_o) and γ -radio loudness (G_r) as $G_o \equiv S'_{\gamma}/S'_{\text{opt}}$ and $G_r \equiv S'_{\gamma}/S'_{\text{VLBA}}$, respectively. We find that the radio luminosity and γ -optical loudness are significantly correlated only for quasars (see Table 1 and Fig. 5, left panel), $L_{\text{VLBA}} \propto G_o^{0.45 \pm 0.12}$.

The correlation in the $L_{\text{opt}} - G_r$ plane (Fig. 5, right panel) is marginally significant only for BL Lacs (Table 1). A large amount of scatter about the fitted line and small sampling of BL Lacs account for the large error of the power index ($L_{\text{opt}} \propto G_r^{-0.81 \pm 0.48}$).

Logarithm of the median γ -optical loudness is significantly different for quasars and BL Lacs (2.1 and 1.2), while there is no difference between their medians of γ -radio loudness (2.1 and 2). There are no high-energy peaked BL Lacs in the MOJAVE-1 sample. The latter have significantly different SED properties than the radio-selected MOJAVE-1 BL Lacs (Lister et al. 2011). The differences found between quasars and BL Lacs are also supported in recent studies (e.g., Ghisellini et al. 2009, Sambruna et al. 2010, Tornikoski et al. 2010, Gupta et al. 2011) suggesting the presence of different physical conditions along the jet in quasars and BL Lacs. This and other insights into the relationship between the γ -ray, radio, and optical emission will be pursued in more detail in further studies.

Relations found between L_{γ} and R , L_{VLBA} and G_o , and L_{opt} and G_r are due to variations of the SED of blazars, which can be driven by changes of the Doppler factor, magnetic field, and intrinsic power of the jets. In the next section, we attempt to identify the main physical parameters of the jet responsible for the observed correlations.

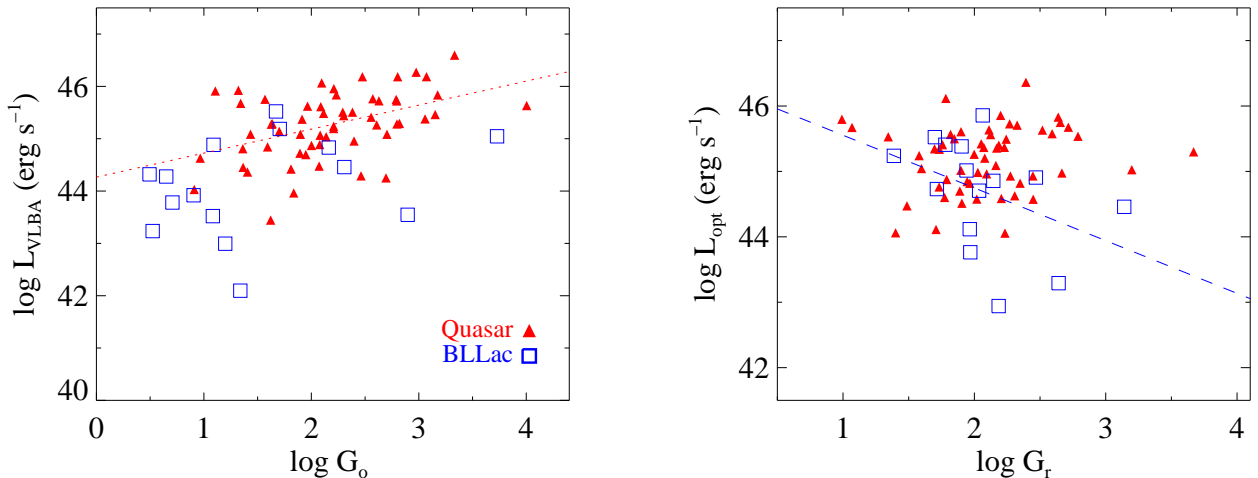


Fig. 5 *Left panel*. Radio VLBA luminosity against γ -optical loudness ($G_o \equiv S'_\gamma/S'_{\text{opt}}$) for the M1-1FGL quasars and BL Lacs. *Right panel*. Optical luminosity against γ -radio loudness ($G_r \equiv S'_\gamma/S'_{\text{VLBA}}$). The dotted and dashed lines represent the ordinary least-square fit to the data for quasars and BL Lacs respectively.

4. Interpretation and model implications

The broadband emission of blazars is generally understood as originating from ultrarelativistic particles in the relativistic jet, which is oriented at a small angle $\theta_{\text{obs}} \sim 1/\Gamma$ (where Γ is the bulk Lorentz factor of the material moving along the jet) with respect to our line of sight. The low-frequency continuum emission from radio to optical – UV (or even X-rays, in high-frequency-peaked BL Lac objects) frequencies is generally accepted to be synchrotron emission from relativistic electrons in the jet. The high-energy (X-ray– γ -ray) emission can be either inverse Compton emission from the same electrons (leptonic models), or emission resulting from the production of secondaries in photo-pair and photo-pion production reactions of ultrarelativistic hadrons in the jet (hadronic models). For a recent review of blazar models, see, e.g., Böttcher (2010).

We will discuss a possible interpretation of the correlations described above, in the framework of a steady-state, one-zone leptonic model. Specifically, we adopt the semi-analytical description of a generic leptonic blazar model of Böttcher & Dermer (2002). In this model, a power-law distribution of relativistic electrons, $Q(\gamma) = Q_0 \gamma^{-q} H(\gamma; \gamma_1, \gamma_2)$ with low- and high-energy cut-offs γ_1 and γ_2 is persistently injected into a spherical emission region of radius R_B , which moves with constant speed $\beta_\Gamma c$, corresponding to bulk Lorentz factor Γ , along the jet. In order to reduce the free parameter space, we choose an observing angle of $\theta_{\text{obs}} = 1/\Gamma$ so that the Doppler factor $D = (\Gamma [1 - \beta_\Gamma \cos \theta_{\text{obs}}])^{-1} = \Gamma$. A tangled magnetic field B is present in the emission region. Modeling of the SEDs of many BL Lac objects indicates that a model including only synchrotron and synchrotron-self-Compton (SSC), is often sufficient to describe those SEDs (e.g., Mastichiadis & Kirk 1997; Pian et al. 1998; Petry et al.

2000; Krawczynski et al. 2002). Therefore, we adopt a pure SSC model in this study to represent the SEDs of high-frequency-peaked blazars (BL Lac objects), which is fully determined through the model parameters listed above. In the model of Böttcher & Dermer (2002), the injected electron distribution is followed in an iterative process to equilibrium between ongoing particle injection and radiative cooling and escape. Fig. 6 shows a characteristic sequence of BL Lac SEDs resulting from a variation of the jet power L_j , while keeping the magnetic field at equipartition with the equilibrium electron distribution. Typical parameters for one of those SED calculations are listed in Table 2.

For low-frequency-peaked BL Lacs (LBLs) and flat-spectrum radio quasars (FSRQs), it is generally accepted that leptonic models require external photon sources for Compton scattering (EC = External Compton) to produce the γ -ray emission (e.g., Dermer et al. 1997; Sambruna et al. 1997; Mukherjee et al. 1999; Madejski et al. 1999; Böttcher & Bloom 2000; Hartman et al. 2001). In the case of quasars, the most prominent external radiation field might be the quasi-isotropic radiation field of the broad-line region (BLR), as long as the emission region is located within the BLR. We model the BLR as a spherical shell at a distance R_{BLR} from the central engine, reprocessing a fraction τ_{BLR} of the accretion disk luminosity, L_D . In this case, the jet power is parameterized as a fraction f_j of the accretion disk luminosity, i.e., $L_j = f_j L_D$. As in the case of BL Lac objects, we assume the persistent injection of a power-law distribution of ultrarelativistic electrons into the emission region, and let the distribution evolve to an equilibrium between injection, radiative cooling, and escape. A typical set of parameters producing an FSRQ-like SED is listed in Table 3. A sequence of FSRQ

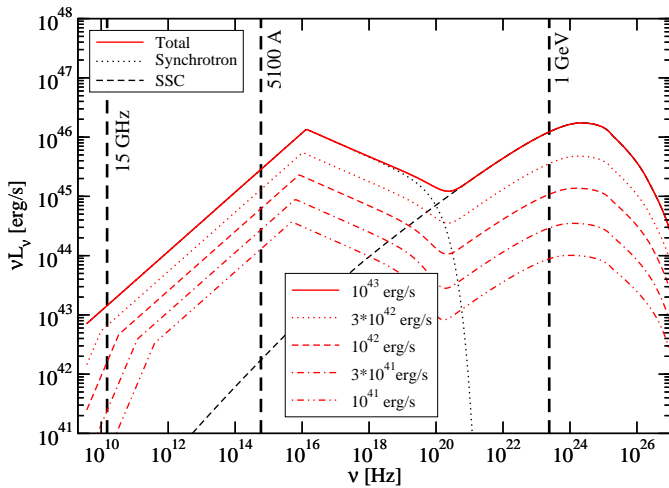


Fig. 6 Sequence of model SEDs for BL Lac objects, varying the jet power, while adjusting the magnetic field to equipartition with the relativistic electrons in the jet. The curves are labelled by the value of L_j . The black dotted and dashed lines indicate the individual radiation components adding up to the the total spectrum with the highest $L_j = 10^{43} \text{ erg s}^{-1}$. This sequence yields the points shown as blue open squares in Figs. 8 – 10 .

SEDs, resulting from a change in the accretion disk power (and hence also the jet power), while adjusting the magnetic field to be in equipartition with the equilibrium electron distribution, is shown in Fig. 7.

We tested whether variations of individual parameters for FSRQs and BL Lacs were able to reproduce the observed statistically significant ($P < 0.05$) correlations between R and L_γ , G_o and L_{VLBA} for quasars, and between G_r and L_{opt} for BL Lacs. In particular, we tested whether these correlations can arise from a change in the following fundamental parameters: (a) Accretion disk (and hence, jet) power L_D (L_j), (b) Accretion disk (and jet) power, while keeping the magnetic field in equipartition with the equilibrium electron distribution ($\epsilon_B \equiv u_B/u_e = 1$), (c) Accretion disk (and jet) power with $\epsilon_B = 1$, adjusting the BLR radius as $R_{\text{BLR}} \propto L_D^{1/2}$, (d) Lorentz factor Γ (and, hence, the Doppler factor D), (e) viewing angle θ_{obs} (also changing the Doppler factor D), and (f) magnetic field B . The resulting theoretical correlations for FSRQs are shown by the filled symbols in Figs. 8 – 10, while open symbols show representative sequences for BL Lac objects. In all cases, we ran one sequence per base parameter. Figs. 8 – 10 show representative results. The straight lines in these figures indicate the best power-law fits to the observed correlations.

When comparing the theoretical correlations with the observed ones, one needs to keep in mind that our model only takes into account radio emission from the high-energy emission region in the sub-pc scale core. Realistically, we expect a substantial contribution to the observed radio emission to arise on larger ($\gtrsim \text{pc}$) scales. Therefore, our model radio fluxes should be considered as

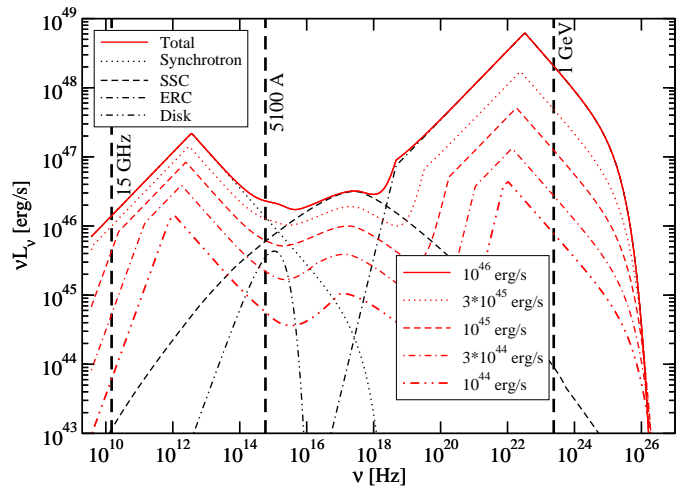


Fig. 7 Sequence of model SEDs for quasars, varying the accretion disk luminosity L_D (and hence, the jet power $L_j = f_j L_D$), while adjusting the magnetic field to equipartition with the relativistic electrons in the jet. The curves are labelled by the value of L_D . The black dotted, dashed, dot-dashed, and dot-dot-dashed lines indicate the individual radiation components adding up to the total spectrum with the highest $L_D = 10^{46} \text{ erg s}^{-1}$. This sequence yields the points shown as blue filled squares in Figs. 8 – 10.

Table 2 Typical leptonic jet model parameters for a BL Lac object.

Quantity	Symbol	Value
Minimum injection electron Lorentz factor	γ_1	10^4
Maximum injection electron Lorentz factor	γ_2	10^6
Electron injection spectral index	q	2.5
Magnetic field	B	2 G
Blob radius	R_B	$3 \times 10^{15} \text{ cm}$
Bulk Lorentz factor	Γ	15
Observing angle	θ_{obs}	3.82°
Jet power	L_j	$10^{42} \text{ erg s}^{-1}$

Table 3 Typical leptonic jet model parameters for a quasar.

Quantity	Symbol	Value
Minimum injection electron Lorentz factor	γ_1	300
Maximum injection electron Lorentz factor	γ_2	10^5
Electron injection spectral index	q	3.1
Magnetic field	B	0.661 G
Blob radius	R_B	10^{17} cm
Bulk Lorentz factor	Γ	15
Observing angle	θ_{obs}	3.82°
Accretion disk luminosity	L_D	$10^{45} \text{ erg s}^{-1}$
Jet power fraction	f_j	0.05
Reprocessing Optical Depth of BLR	τ_{BLR}	0.1
Effective radius of BLR	R_{BLR}	10^{18} cm

lower limits. In particular, additional radio emission from larger scales would shift all model curves to the right in Fig. 8 and to the left in Fig. 9. Considering this potential offset, we identified a set of parameters with which the observed R vs. L_γ (Fig. 8), G_r vs. L_{opt} (Fig. 9), and G_o vs. L_{VLBA} (Fig. 10) correlations can be reasonably well reproduced through a variation of L_D (and L_j), while keeping the magnetic field in equipartition with the electron distribution. Those sequences are marked by the blue dashed line (square symbols) in Figs. 8 – 10, and the sequences of SEDs are illustrated in Figs. 6 and 7 for typical pa-

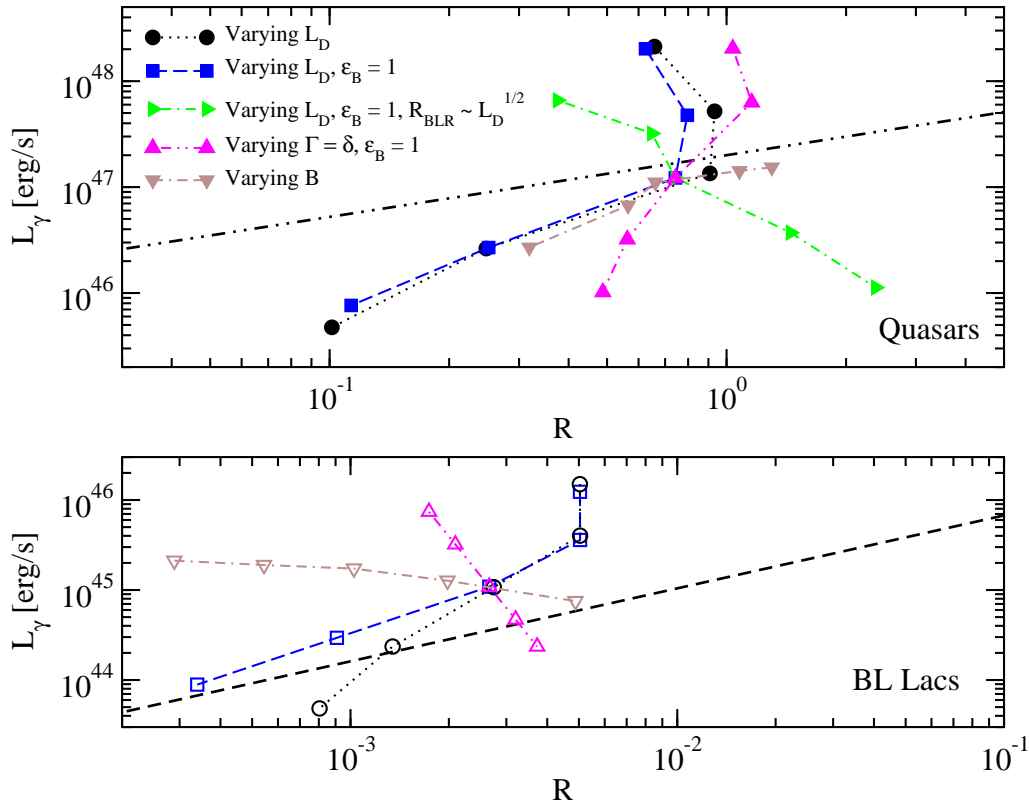


Fig. 8 Model correlations of radio-optical loudness R vs. gamma-ray luminosity L_γ along sequences varying individual parameters. Each sequence represents the effect of a variation of one individual base parameter. The legend in the top left indicates the parameters varied along the sequences. Filled symbols indicate SEDs characteristic of FSRQs, while open symbols indicate sequences of SEDs characteristic of BL Lacs. The long-dashed and dot-dot-dashed lines mark the power-law correlations that best fit the observational data. The sequences marked in blue dashed line (squares), showing reasonable agreement with the best-fit correlations, correspond to the sequences of SEDs shown in Figs. 6 and 7 (see also Tables 2 and 3).

parameters of the jet in BL Lacs and quasars (Tables 2 and 3). Most other parameter sequences produce correlations with opposite slopes than observed, while a variation of only the magnetic field over about two orders of magnitude results in too small a range in radio-optical loudness to be consistent with the observed correlations (downward triangles in Fig. 8).

However, while reasonable agreement can be achieved with the R vs. L_γ correlation for quasars and BL Lacs and G_r vs. L_{opt} correlation for BL Lacs, our favored sequence of changing L_D (L_j) with $\epsilon_B \equiv 1$ predict steep-slope positive correlations between G_o and L_{VLBA} for quasars, in discrepancy with the slope of the observed positive correlation (Fig. 5; left panel). A better agreement is achieved for changes of the accretion power L_D and the Lorentz factor of the jet (black circles and downward triangles in Fig. 10). We therefore conclude that a simple one-parameter sequence is not able to reproduce the observational results. The substantial scatter in all correlations also might be an indication that those are not single-parameter sequences. In a realistic scenario, we expect that a combination of different parameter variations and physical relations between parameters are responsible for the observed range of

radio, optical, and γ -ray luminosities. To disentangle the effect of multiple parameter sequences it is essential to provide information on individual parameters (e.g. variance in Lorentz factor, variance in B field, etc.) from further studies. Moreover, the dispersion of the observed correlations can be used to constrain the distribution of initial parameters of the model. For this purpose, (quasi-) simultaneous observations of the SED (from radio to γ -ray) of more than 100 blazars (Planck Collaboration et al. 2011; Giommi et al. 2011) may be used to test the found correlations and to constrain further the jet model. This will be presented in a subsequent paper.

Predictions of the model sequences are presented for quasars in Fig. 9 (top panel) and BL Lacs in Fig. 10 (empty symbols). These can be tested with significant $L_{\text{opt}} - G_r$ and $L_{\text{VLBA}} - G_o$ correlations derived from larger samples of blazars.

5. Summary

Using the sample of 78 core dominated blazars (59 quasars and 19 BL Lacs) detected by *Fermi*/LAT from the MOJAVE-1 sample, we investigate the relations between

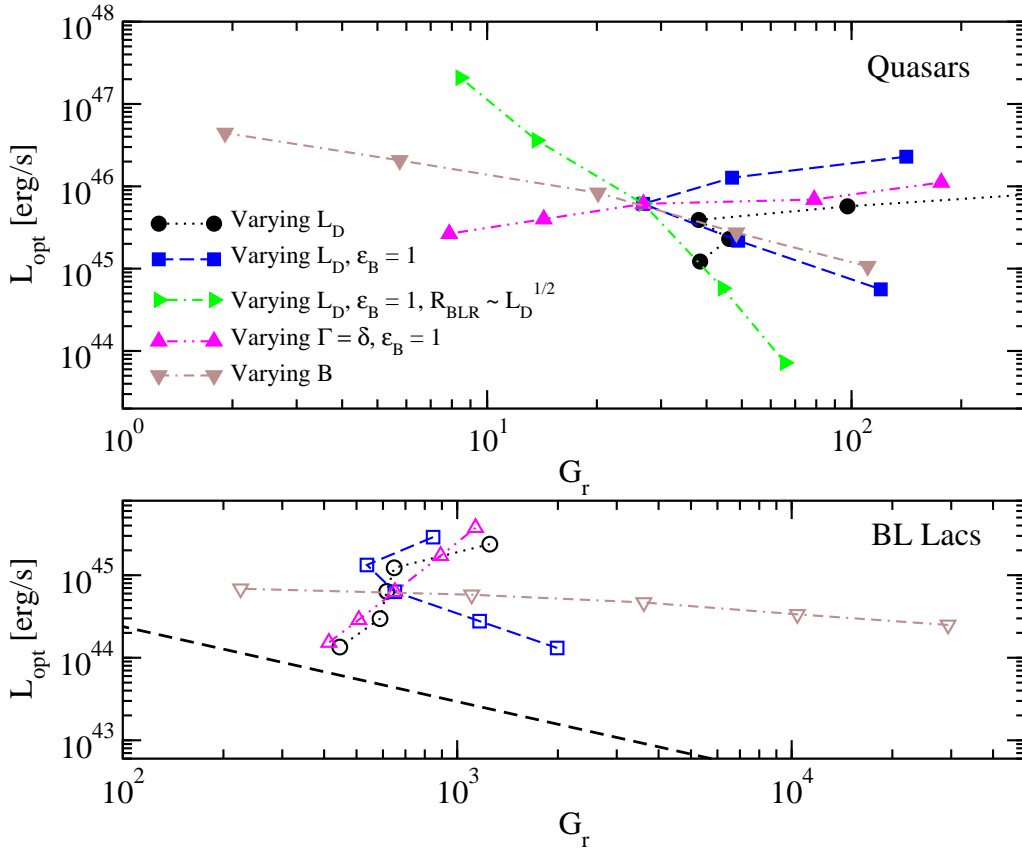


Fig. 9 Model correlations of the γ -ray-to-radio flux ratio vs. optical luminosity along sequences varying individual parameters. Each sequence represents the effect of a variation of one individual base parameter. The legend in the top left indicates the parameters varied along the sequences. Filled symbols indicate SEDs characteristic of FSRQs, while open symbols indicate sequences of SEDs characteristic of BL Lacs. The long-dashed line marks the power-law correlation that best fits the observational data. The sequences marked in blue dashed line (squares) correspond to the sequences of SEDs shown in Figs. 6 and 7 (see also Tables 2 and 3).

their radio, optical, and γ -ray emission available from non-simultaneous observations. Our main results are summarized as follows:

- The detection rate of the γ -ray blazars from the radio-selected MOJAVE-1 sample is high for radio bright blazars and it is independent of their optical nuclear fluxes. Most of non-detected γ -ray blazars are radio weak quasars. They are optically faint but also very luminous, $L_{\text{opt}} > 10^{44.5}$ erg s $^{-1}$.
- The known correlation between γ -ray flux and compact radio flux density (measured quasi-simultaneously) is also valid for non-simultaneous measurements of L_γ and L_{VLBA} for 59 quasars and 19 BL Lacs. This indicates that the Doppler-factors of the jet-plasma in the gamma and radio regimes are fairly constant on a timescale of a few years. The $L_\gamma - L_{\text{VLBA}}$ correlation is significantly stronger than that in the $L_\gamma - L_{\text{opt}}$ plane. The latter holds exclusively for quasars at the confidence level (c.l.) of 98.9%. The relation $\log L_{\text{VLBA}} = (0.83 \pm 0.03) \log L_\gamma + (5.96 \pm 0.26)$ can be used as a predictor of γ -ray flux from radio flux density at 15 GHz.
- We report a statistically significant positive correlation ($> 99\%$) between γ -ray luminosity and radio-optical loudness ($R \propto S_{\text{VLBA}}/S_{\text{opt}}$) for both quasars and BL Lacs.
- Radio-optical loudness and γ -optical loudness of the population of quasars is one order of magnitude larger than those of BL Lacs, while no difference is found between γ -radio loudness of two populations.
- We find a correlation between radio luminosity at 15 GHz and γ -ray-optical loudness ($G_o \propto S_\gamma/S_{\text{opt}}$) for quasars, $L_{\text{VLBA}} \propto G_o^{0.45 \pm 0.12}$ (c.l. $> 99.99\%$). The relationship between γ -ray-radio loudness ($G_r \propto S_\gamma/S_{\text{VLBA}}$) and optical nuclear luminosity is marginally significant for BL Lacs ($L_{\text{opt}} \propto G_r^{-0.81 \pm 0.38}$; c.l. 95.8%) with a large error in the power index.
- We employ the generic leptonic model for blazars to reproduce the observed correlations between γ -ray emission, optical, and radio emission described above. Among all parameters of the jet model, only a variation of the accretion power (and the jet power) — with the magnetic field in equipartition with relativis-

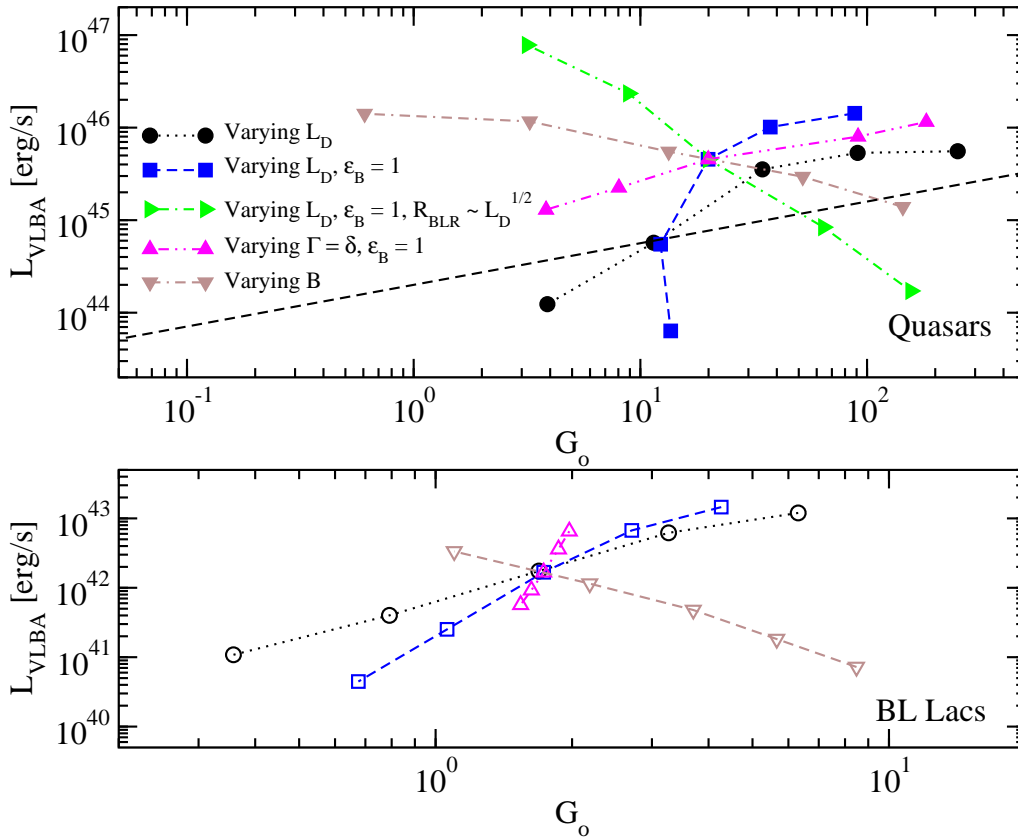


Fig. 10 Model correlations of the γ -ray-to-optical flux ratio vs. radio luminosity along sequences varying L_D (for quasars, with $f_j = \text{const.}$) and L_j (for BL Lacs), keeping the magnetic field at equipartition (squares), and varying B (downward triangles). Filled symbols indicate SEDs characteristic of FSRQs, while open symbols indicate sequences of SEDs characteristic of BL Lacs. The sequences marked in blue dashed line (squares) correspond to the sequences of SEDs shown in Figs. 6 and 7.

tic electrons in the jet — can reasonably well reproduce the observed strong correlations between L_γ and R for quasars and BL Lacs, L_{opt} and G_r for BL Lacs, and L_{VLBA} and G_o for quasars. We conclude that the change of the accretion (and jet) power is the main parameter responsible for the trends in most of the observed correlations but a combination of variations of the accretion power with other jet parameters such as the jet viewing angle, Lorentz factor, and the magnetic field is needed to fit all correlations. Independent variations of the latter parameters will open up too large a parameter space, which makes infeasible the consideration of all possible combinations of parameter variations in this work. A larger sample of blazars, which will include the faint end of the population, is needed to better constrain the correlations between the bands. Ideally, one would need a simultaneous multi-band monitoring of a larger sample of blazars to test different jet models.

Acknowledgements. We thank the MOJAVE team members for useful discussions. T.G.A. acknowledges support by DFG-SPP project under grant 566960. E.R. acknowledges partial support by the Spanish MICINN through grant AYA2009-13036-C02-02. This work was supported by

CONACYT research grants 54480 and 151494 (México), NASA through Fermi Guest Investigator Program award NNX09AT82G and Astrophysics Theory Program Award NNX10AC79G. The MOJAVE project is supported under National Science Foundation grant 0807860-AST and NASA-Fermi grant NNX08AV67G. The VLBA is operated by the National Radio Astronomy Observatory a facility of the National Science Foundation operated under cooperative agreement by Associated Universities, Inc.

References

- Abdo, A. A., Ackermann, M., Ajello, M., et al. 2010a, *Nature*, 463, 919
- Abdo, A. A., Ackermann, M., Ajello, M., et al. 2010b, *ApJS*, 188, 405
- Akritis, M. G., & Siebert, J. 1996, *MNRAS*, 278, 919
- Arshakian, T. G., León-Tavares, J., Lobanov, A. P., et al. 2010a, *MNRAS*, 401, 1231
- Arshakian, T. G., Torrealba, J., Chavushyan, V. H., et al. 2010b, *A&A*, 520, 62
- Böttcher, M., 2010, in proc. of “Fermi Meets Jansky”, MPIfR, Bonn, Eds. T. Savolainen, E. Ros, R. W. Porcas, & J. A. Zensus, p. 41
- Böttcher, M., & Dermer, C. D., 2002, *ApJ*, 564, 86

- Böttcher, M., & Bloom, S. D., 2000, *AJ*, 119, 469
- Dermer, C. D., Sturmer, S. J., & Schlickeiser, R., 1997, *ApJS*, 109, 103
- Fichtel, C. E., Bertsch, D. L., Chiang, J., et al. 1994, *ApJS*, 94, 551
- Ghirlanda, G., Ghisellini, G., Tavecchio, F., Foschini, L., & Bonnoli, G. 2011, *MNRAS*, 413, 852
- Ghisellini, G., Maraschi, L., & Tavecchio, F. 2009, *MNRAS*, 396, L105
- Giommi, P., Polenta, G., Lahteenmaki, A., et al. 2011, submitted to *A&A*, arXiv:1108.1114
- Gupta, J. A., Browne, I. W. A., & Peel, M. W. 2011, submitted to *MNRAS*, arXiv:1106.5172
- Hartman, R. C., Böttcher, M., Aldering, G., et al. 2001, *ApJ*, 553, 683
- Kellermann, K. I., Vermeulen, R. C., Zensus, J. A., & Cohen, M. H. 1998, *AJ*, 115, 1295
- Krawczynski, H., Coppi, P. S., & Aharonian, F. 2002, *MNRAS*, 336, 721
- Kovalev, Y. Y., Kellermann, K. I., Lister, M. L., et al. 2005, *AJ*, 130, 2473
- Kovalev, Y. Y., Aller, H. D., Aller, M. F., et al. 2009, *ApJ*, 696, L17
- León-Tavares, J., Lobanov, A. P., Chavushyan, V. H., et al. 2010, *ApJ*, 715, 355
- Leon-Tavares, J., Valtaoja, E., Tornikoski, M., Lahteenmaki, A., & Nieppola, E. 2011, arXiv:1102.1290
- Linford, J. D., et al. 2011, *ApJ*, 726, 16
- Lister, M. L., & Homan, D. C. 2005, *ApJ*, 130, 1389
- Lister, M., Aller, H. D., Aller, M. F., et al. 2009a, *AJ*, 137, 3718
- Lister, M. L., Homan, D. C., Kadler, M., et al. 2009b, *ApJL*, 696, L22
- Lister, M. L., Aller, M., Aller, H., et al. 2011, *ApJ*, in press, arXiv:1107.4977
- Madejski, G., Sikora, M., Jaffe, T., et al. 1999, *ApJ*, 521, 145
- Mahony, E. K., Sadler, E. M., Murphy, T., et al. 2010, *ApJ*, 718, 587
- Marscher, A. P., & Gear, W. K. 1985, *ApJ*, 298, 114
- Marscher, A. P., & Jorstad, S. G. 2010, in proc. of “Fermi Meets Jansky”, MPIfR, Bonn, Eds. T. Savolainen, E. Ros, R. W. Porcas, & J. A. Zensus, p. 171, arXiv:1005.5551
- Mastichiadis, A., & Kirk, J. G. 1997, *A&A*, 320, 19
- Mukherjee, R., Böttcher, M., Hartman, R. C., et al. 1999, *ApJ*, 527, 132
- Petry, D., Böttcher, M., Connaughton, V., et al. 2000, *ApJ*, 536, 742
- Pian, E., Vacanti, G., Tagliaferri, G., et al. 1998, *ApJ*, 492, L17
- Planck Collaboration, et al. 2011, arXiv:1101.2047
- Pushkarev, A. B., Kovalev, Y. Y., & Lister, M. L. 2010, *ApJ*, 722, L7
- Sambruna, R. M., Donato, D., Ajello, M., et al. 2010, *ApJ*, 710, 24
- Sambruna, R. M., Urry, C. M., Maraschi, L., et al. 1997, *ApJ*, 474, 639
- Tornikoski, M., Nieppola, E., Valtaoja, E., León-Tavares, J. & Lähteenmäki, A. 2010, in proc. of “Fermi Meets Jansky”, MPIfR, Bonn, Eds. T. Savolainen, E. Ros, R. W. Porcas, & J. A. Zensus, p. 85
- Zensus, J. A., Ros, E., Kellermann, K. I., et al. 2002, *AJ*, 124, 662

Table 4. Optical, radio, and γ -ray parameters of the 76 AGN from the MOJAVE-1 sample. Column (1) is the IAU 1950.0 name of the object; (2) is the optical spectral type: quasars (Q), BL Lacs (BL), and radio galaxies (G); (3) is the redshift; (4) is the logarithm of the total radio flux (radio flux density multiplied by 15 GHz) in units of $\text{erg s}^{-1} \text{cm}^{-2}$; (5) is the logarithm of the nuclear optical flux (optical flux density multiplied by 5100 Å) in units of $\text{erg s}^{-1} \text{cm}^{-2}$; (6) is the logarithm of the γ -ray energy flux between 0.1-100 GeV in units of $\text{erg s}^{-1} \text{cm}^{-2}$; (7) is the logarithm of the radio luminosity at 15 GHz in units of erg s^{-1} ; (8) is the logarithm of the nuclear optical luminosity at 5100 Å in units of erg s^{-1} ; (9) is the logarithm of the γ -ray luminosity in units of erg s^{-1} . All fluxes are *K*-corrected.

Name (1)	Sp. type (2)	z (3)	$\log S'_{\text{VLBA}}$ (4)	$\log S'_{\text{opt}}$ (5)	$\log S'_{\gamma}$ (6)	$\log L_{\text{VLBA}}$ (7)	$\log L_{\text{opt}}$ (8)	$\log L_{\gamma}$ (9)
0059+581	Q	0.644	-12.29	-12.67	-10.27	44.96	44.58	46.97
0106+013	Q	2.099	-12.34	-12.89	-9.82	46.19	45.63	48.70
0109+224	BL	0.265	-12.81	-11.42	-10.34	43.52	44.91	45.99
0133+476	Q	0.859	-12.12	-12.19	-9.89	45.44	45.37	47.67
0202+149	Q	0.405	-12.51	-13.82	-11.13	44.25	42.94	45.63
0202+319	Q	1.466	-12.46	-12.02	-10.68	45.68	46.12	47.46
0212+735	Q	2.367	-12.38	-13.29	-10.31	46.27	45.37	48.34
0215+015	Q	1.715	-12.84	-13.33	-10.18	45.46	44.98	48.13
0234+285	Q	1.207	-12.20	-12.83	-10.04	45.72	45.09	47.89
0235+164	BL	0.940	-12.61	-13.20	-9.47	45.05	44.46	48.19
0316+413	G	0.018	-11.80	-10.35	-9.76	42.06	43.51	44.09
0336-019	Q	0.852	-12.46	-12.14	-10.70	45.09	45.41	46.84
0403-132	Q	0.571	-12.67	-12.24	-10.88	44.45	44.88	46.24
0415+379	G	0.049	-12.05	-12.60	-10.99	42.69	42.14	43.76
0420-014	Q	0.914	-11.79	-12.29	-10.05	45.84	45.34	47.57
0422+004	BL	0.310	-12.57	-11.76	-10.85	43.92	44.73	45.63
0458-020	Q	2.286	-12.43	-13.01	-10.53	46.18	45.61	48.08
0528+134	Q	2.070	-11.91	-13.25	-9.91	46.60	45.26	48.60
0529+075	Q	1.254	-12.69	-13.04	-10.24	45.28	44.93	47.73
0529+483	Q	1.162	-12.80	-13.30	-10.59	45.09	44.59	47.29
0605-085	Q	0.872	-12.54	-12.73	-10.59	45.04	44.85	46.98
0736+017	Q	0.191	-12.56	-11.95	-10.33	43.45	44.06	45.68
0748+126	Q	0.889	-12.32	-12.25	-10.62	45.28	45.35	46.97
0754+100	BL	0.266	-12.55	-11.32	-10.61	43.78	45.01	45.72
0805-077	Q	1.837	-12.62	-12.55	-9.98	45.76	45.83	48.40
0808+019	BL	1.148	-12.69	-12.49	-10.78	45.19	45.38	47.09
0814+425	BL	0.245	-12.71	-12.96	-10.06	43.55	43.29	46.19
0823+033	BL	0.506	-12.67	-11.47	-10.97	44.32	45.52	46.02
0827+243	Q	0.940	-12.51	-12.09	-10.39	45.14	45.56	47.27
0829+046	BL	0.174	-12.68	-11.06	-10.54	43.24	44.86	45.38
0836+710	Q	2.218	-12.52	-12.22	-10.12	46.07	46.36	48.46
0838+133	Q	0.681	-12.94	-12.32	-10.92	44.36	44.99	46.39
0851+202	BL	0.306	-12.20	-11.07	-10.42	44.28	45.41	46.06
0906+015	Q	1.024	-12.38	-12.02	-10.11	45.37	45.73	47.64
0917+624	Q	1.446	-12.86	-13.19	-10.58	45.26	44.93	47.54
1055+018	Q	0.890	-12.09	-12.39	-10.01	45.51	45.20	47.59
1124-186	Q	1.048	-12.36	-12.95	-10.40	45.41	44.82	47.38
1127-145	Q	1.184	-12.28	-12.05	-10.08	45.62	45.86	47.82
1156+295	Q	0.729	-12.30	-12.02	-10.13	45.09	45.36	47.26
1219+044	Q	0.965	-12.84	-12.19	-10.60	44.84	45.49	47.09
1222+216	Q	0.432	-12.86	-12.25	-10.42	43.96	44.58	46.41
1226+023	Q	0.158	-11.35	-11.71	-9.64	44.48	44.11	46.19
1228+126	G	0.004	-12.39	-9.78	-10.76	40.14	42.76	41.78
1253-055	Q	0.536	-11.55	-11.65	-9.36	45.51	45.40	47.69
1308+326	Q	0.997	-12.34	-13.09	-10.03	45.38	44.63	47.69
1324+224	Q	1.400	-13.02	-12.51	-10.43	45.07	45.58	47.66
1334-127	Q	0.539	-11.86	-12.59	-10.38	45.19	44.47	46.68

Table 4. continued.

Name (1)	Sp. type (2)	z (3)	S'_{VLBA} (4)	S'_{opt} (5)	S'_{γ} (6)	$\log L_{\text{VLBA}}$ (7)	$\log L_{\text{opt}}$ (8)	$\log L_{\gamma}$ (9)
1502+106	Q	1.839	-12.75	-13.08	-9.08	45.63	45.30	49.30
1510-089	Q	0.360	-12.35	-11.61	-9.15	44.29	45.03	47.49
1546+027	Q	0.414	-12.36	-12.27	-10.46	44.42	44.51	46.33
1548+056	Q	1.422	-12.35	-12.58	-11.01	45.75	45.53	47.10
1606+106	Q	1.226	-12.46	-12.52	-10.41	45.48	45.42	47.54
1611+343	Q	1.397	-12.16	-12.41	-11.09	45.93	45.67	46.99
1633+382	Q	1.814	-12.18	-12.66	-9.86	46.19	45.71	48.51
1641+399	Q	0.593	-11.87	-11.66	-10.02	45.29	45.50	47.14
1726+455	Q	0.717	-12.47	-12.66	-10.58	44.89	44.70	46.78
1730-130	Q	0.902	-11.77	-13.55	-10.37	45.84	44.06	47.24
1749+096	BL	0.322	-12.07	-12.41	-10.10	44.46	44.12	46.42
1803+784	BL	0.680	-12.42	-11.45	-10.36	44.88	45.86	46.95
1807+698	BL	0.051	-12.68	-11.84	-10.50	42.10	42.94	44.28
1823+568	BL	0.664	-12.45	-12.58	-10.41	44.83	44.71	46.87
1828+487	Q	0.692	-12.70	-12.08	-11.12	44.63	45.24	46.21
1849+670	Q	0.657	-12.57	-11.73	-9.78	44.70	45.54	47.49
1958-179	Q	0.650	-12.39	-12.29	-10.29	44.87	44.96	46.96
2131-021	BL	1.285	-12.47	-12.76	-11.08	45.52	45.24	46.91
2145+067	Q	0.990	-11.80	-11.91	-10.81	45.91	45.80	46.90
2155-152	Q	0.672	-12.48	-12.25	-10.89	44.81	45.04	46.41
2200+420	BL	0.069	-12.06	-11.29	-10.09	42.99	43.76	44.96
2201+171	Q	1.076	-12.51	-12.98	-10.16	45.29	44.82	47.64
2209+236	Q	1.125	-12.61	-13.09	-10.88	45.24	44.76	46.97
2223-052	Q	1.404	-12.13	-12.52	-10.31	45.96	45.57	47.78
2227-088	Q	1.560	-12.48	-12.46	-9.83	45.72	45.75	48.38
2230+114	Q	1.037	-12.15	-12.13	-10.04	45.61	45.64	47.72
2251+158	Q	0.859	-11.81	-11.88	-9.09	45.75	45.68	48.47
2331+073	Q	0.401	-12.72	-11.73	-10.82	44.03	45.02	45.93
2345-167	Q	0.576	-12.41	-12.53	-10.63	44.72	44.60	46.50